SIAM J. SCI. COMPUT.
Vol. 33, No. 5, pp. 2536–2559

GEOMETRIC PROPERTIES OF THE ICOSAHEDRAL-HEXAGONAL GRID ON THE TWO-SPHERE*

NING WANG† AND JIN-LUEN LEE‡

Abstract. An icosahedral-hexagonal grid on the two-sphere is created by dividing the faces of an icosahedron and projecting the vertices onto the sphere. This grid and its Voronoi tessellation have several desirable features for numerical simulations of physical processes on the sphere. While several methods to construct the icosahedral grid mesh have been proposed over the past decades, and empirical data have been collected to understand and help improve the grid, rarely have analytical analyses been done to investigate the basic geometric properties of the grid. In this paper, we present an analytical analysis of several geometric properties of the icosahedral grids based on two basic constructions: recursive and nonrecursive construction. We point out that these geometric properties can be improved with modified construction procedures. We demonstrate how these improvements impact the numerical integration of PDEs over the sphere.

Key words. icosahedral grid, Voronoi tessellation, shallow water model

AMS subject classifications. 65M50, 65N50, 65M60

DOI. 10.1137/090761355

1. Introduction.

An icosahedral-hexagonal grid on the two-sphere is created by dividing the faces of an icosahedron (which are 20 congruent equilateral plane triangles) into a triangle mesh and projecting the vertices of the mesh onto the surface of the enclosing sphere. Its relevant topology includes a mesh of triangles and hexagonal Voronoi cells (and 12 pentagonal ones) that provide a unique set of geometric properties suitable for numerical simulations on the sphere. Among all regular polyhedrons, the icosahedron distributes the 4π angular defect (Gauss–Bonnet theorem) evenly over the most number of vertices, minimizing the distortion of the spherical triangles near these vertices. In addition, an icosahedral grid partitions the sphere into 20 equilaterals, which naturally leads to 10 rhombuses that can be further decomposed conveniently for massive parallel computing. Due to these desirable geometric and topological features, several discretization schemes have been developed based on the icosahedral-hexagonal grid for global circulation models ([1, 9, 8, 6, 16], for example).

Figure 1.1 shows 20 initial equilateral plane triangles that can be combined into an icosahedron.

There are two basic constructions for this grid: one is recursive and one nonrecursive. We will describe both constructions in detail in the following sections. In general, the grid points created from either construction are rather uniform. However, we know that for more than 12 grid points it is impossible to create a perfect grid mesh on the sphere, which requires equal distance between any adjacent grid points. Therefore, there is a need to specify some measures of grid regularity and to optimize these measures during the construction process. Several criteria have been suggested,

*Submitted to the journal's Methods and Algorithms for Scientific Computing section June 5, 2009; accepted for publication (in revised form) June 13, 2011; published electronically October 18, 2011.

http://www.siam.org/journals/sisc/33-5/76135.html

†Cooperative Institute for Research in the Atmosphere, Colorado State University, and NOAA Earth System Research Laboratory, 325 Broadway, R/GSD6, Boulder, CO 80305 (ning.wang@noaa.gov).

‡NOAA Earth System Research Laboratory, 325 Broadway, R/OD, Boulder, CO 80305 (jin.lee@noaa.gov).

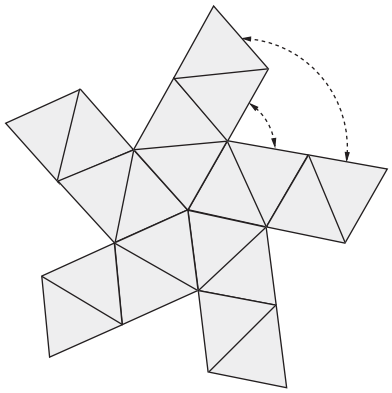

FIG. 1.1. *Initial* 20 *equilateral plane triangles that form the regular icosahedron.*

and corresponding iterative procedures have been proposed [17, 3] to optimize the grid. However, little has been done to analytically study the geometric properties of the grid and to demonstrate the impact of these optimizations on the grid geometrically. The purpose of this study is to analytically investigate the structure of the icosahedral grid, providing geometric insight into the grid to help improve the numerical qualities of the grid for various applications.

There are two key parameters that are most important to a spherical grid. The first is the regularity of the triangle mesh and its corresponding Voronoi cell mesh. It directly affects the truncation error of the numeric computation performed on it [3, 17]. The bound of the regularity may be measured with the maximum ratio between the longest and the shortest side of any spherical triangle in the triangle mesh. The overall regularity of the grid may be measured by the variance of the Voronoi cell edges or that of the grid point spacing. The second parameter is the uniformity of the triangle mesh, which is commonly measured by the ratio of the longest and shortest distances between any adjacent grid points. This parameter determines the size of the time step for numerical integration of time-dependent hyperbolic equations. It is especially important when a high resolution grid is used and computational efficiency becomes a critical factor.

In their survey paper [10], Miura and Kimoto summarized several iterative optimization methods. They identified the following five measures that are important to the accuracy of the numerical computation on an icosahedral grid: (i) "collocation" (of the centroids and generators of the Voronoi cells); (ii) "orthogonality"; (iii) "bisection" (conditions for Voronoi cell edges and connections between corresponding grid points); (iv) "isotropy"; and (v) "area uniformity" (of the Voronoi cells). We realize that measures (i)–(iv) are all directly connected to the grid regularity parameter, measure (ii) is always maintained if we do not relocate the generators, and measure (v) is directly related to the ratio of the longest and shortest distances between adjacent grid points. We believe that the two parameters we proposed above are key measures of the grid quality.

It appears that the two key parameters may not simultaneously achieve their optimality. Some compromises have to be made to create a grid that best fits one's particular numerical computation goals. Iterative methods tend to optimize one particular parameter; however, they lack the flexibility for achieving a desired compromise.

In this paper, we analytically determine some key geometric properties of the icosahedral grid that are related to the above parameters. Using these geometric

properties, we determine how skewed and uneven these grids become as their resolution goes to infinity. At the same time, these properties help reveal the weaknesses of the icosahedral grids created from the two basic constructions and find modifications to the constructions that create improved grids for numerical applications.

This article is organized as follows. In section 2, we introduce the basic procedures used to create the icosahedral grid and some notation for the following sections. Section 3 studies the geometric properties of the grid, providing details of the analysis and presenting the analysis results. From these results, we propose two modifications for recursive and nonrecursive construction, respectively, in section 4. In section 5, we present the numerical results from a shallow water model integration over the modified grids and compare them to the same numerical computation over the grid from the basic construction. We conclude the article with some remarks about grid generation on the two-sphere.

2. Construction of the icosahedral grid. There are two basic ways to construct an icosahedral grid: recursive construction and nonrecursive construction. Recursive construction bisects, projects, and subdivides the initial 20 plane equilateral triangles and repeats the procedure on the subdivided plane triangles recursively to create a grid of desired resolution. It is the construction most researchers use at the present time. The nonrecursive construction subdivides the 20 initial plane equilateral triangles, then projects the intersection points onto the surface of the sphere. Sadourny. Arakawa, and Mintz proposed a nonrecursive construction when they introduced their icosahedral grid [13]. Recently, Steppeler et al. proposed a new nonrecursive construction based on dividing a bilinear surface of two adjacent initial plane triangles [14]. Here, we present a slightly different, simple algorithm as our baseline for nonrecursive construction. The nonrecursive construction is a less widely used way to create icosahedral grids; however, this construction produces some desirable geometric properties that could be useful for some numerical applications.

Since all 20 initial plane triangles are congruent, and the subdivision procedures applied to them are exactly the same (except for locally nested or stretched grids which are not dealt with in this article), we can always focus on one such triangle during our descriptions for grid construction, analysis, and proposed modifications. In the following, triangles defined in the three-dimensional ambient Euclidean space are referred to as plane triangles, and triangles defined on the two-sphere are referred to as spherical triangles, or triangles when the context of reference is clear. The Voronoi cells are always defined on the two-sphere.

2.1. Recursive approach. This approach starts with 12 grid points that are evenly distributed on the sphere, with the exact same distance between any adjacent points. Connecting these grid points, we get 20 initial equilateral plane triangles which make up an icosahedron. As one recursively bisects each plane triangle, projects the bisecting points to the sphere, and connects the projected bisecting points to create new triangles, new grid points are added into the grid mesh. The construction is completed when the average (or maximum) distance between adjacent grid points reaches the desired value. The level of recursion is usually called "grid refinement level," or "grid level." The bisection refinement can be equivalently done by bisecting the spherical triangle and connecting the bisecting points with great circles.

For the ease of description, we use the following names and notation. We call the 20 congruent spherical equilateral triangles the initial triangles, or triangles at level 0, and we call these 12 initial evenly spaced grid points the initial vertices, or vertices at level 0. Grid level i refers to the resolution level of the grid after the ith bisection

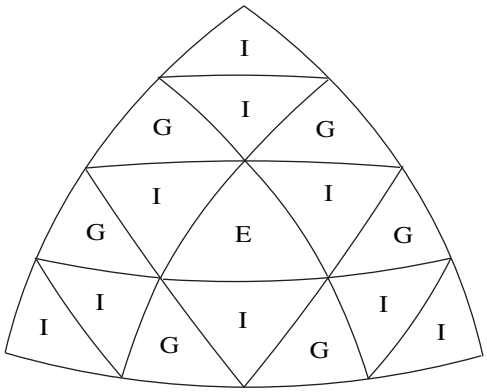

FIG. 2.1. *Recursively bisected equilateral triangle in two levels, letters E, I, and G representing spherical equilateral, isosceles, and general triangles, respectively.*

refinement. We always work on the unit sphere, with all angles and arc lengths in radians.

It is easy to verify that each initial equilateral triangle has a side length of $2\cos^{-1}(1/2 \cdot \csc\frac{\pi}{5})$, angle of $2\pi/5$, and area of $\pi/5$.

The triangle mesh is symmetric with respect to the center of the initial triangle. The triangles at grid level $i\,(i > 0)$ are generally noncongruent. From basic spherical geometry, we have the following patterns. Bisecting and subdividing a spherical equilateral triangle, one will get three spherical isosceles and one spherical equilateral triangle. Bisecting and subdividing a spherical isosceles triangle, one will get two spherical isosceles triangles and two general spherical triangles. Therefore it is trivial to derive the following results. Letting E_n, I_n, and G_n denote the number of spherical equilateral, isosceles, and general triangles at grid level n, we have

$$\begin{aligned} &E_0 = 20, \quad I_0 = 0, \quad G_0 = G_1 = 0,\\ &E_n = E_{n-1}, \quad n > 0,\\ &I_n = I_{n-1} \cdot 2 + E_{n-1} \cdot 3, \quad n > 0,\\ &G_n = G_{n-1} \cdot 4 + I_{n-1} \cdot 2, \quad n > 1. \end{aligned}$$

Or, we have

$$\begin{aligned} &E_0 = 20, \quad I_0 = 0, \quad G_0 = G_1 = 0,\\ &E_n = 20,\\ &I_n = 60(2^n - 1), \quad n > 0,\\ &G_n = 40(2 \cdot 4^{n-1} - 3 \cdot 2^{n-1} + 1), \quad n > 1. \end{aligned}$$

Figure 2.1 shows an initial triangle at level 2 refinement, with letters E, I, and G representing equilateral, isosceles, and general triangles, respectively.

These spherical triangles generally differ in size and side ratios. The ratio between the longest and shortest sides in the triangle mesh increases with the grid level n, and it converges to about 1.195114. Details are discussed in the next section.

The Voronoi cell mesh can be viewed as a complementary mesh to the triangle mesh. There are $10 \cdot 2^{2n} + 2$ grid points, and thus the same number of Voronoi cells. Since the ratio bound of the longest and shortest Voronoi cell edges does not approach

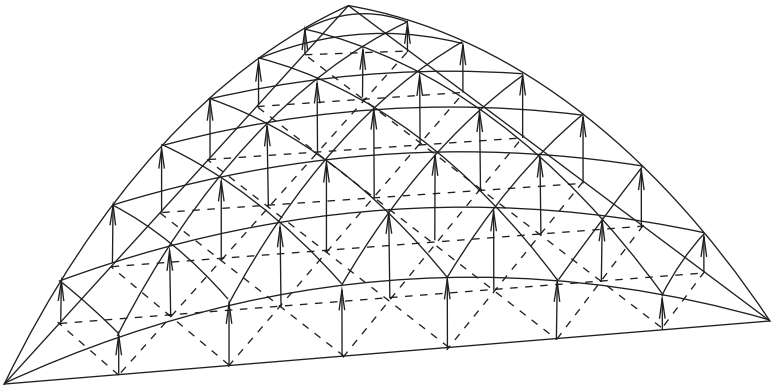

FIG. 2.2. *Nonrecursive construction, each side of the initial equilateral triangle divided into seven equal sections.*

infinity, there are no degenerate spherical pentagons or hexagons. Thus, there are 12 spherical pentagons and $10 \cdot 2^{2n} - 10$ hexagons. Let ν_n and μ_n denote the number of vertices and edges of this mesh. It is straightforward to calculate that

$$\nu_n = \frac{5 \cdot 12 + 6 \cdot (10 \cdot 2^{2n} - 10)}{3} = 20 \cdot 2^{2n},$$
$$\mu_n = \frac{5 \cdot 12 + 6 \cdot (10 \cdot 2^{2n} - 10)}{2} = 30 \cdot 2^{2n}.$$

Recursive construction offers some desirable geometric properties. It provides a good ratio of the longest and shortest distances between adjacent grid points. With a modified construction proposed in section 4, this ratio can be improved to be close to optimality.

The main weakness of this construction is that during the recursive refinements, many local minimum and maximum triangles are created. As a result, in the area near the vertices of the triangles of the first two or three refinements, there are many "skewed" triangles and Voronoi cells.

2.2. Nonrecursive approach. Another basic construction method is nonrecursive. Starting from 12 equally distributed grid points on the sphere, we create 20 plane equilateral triangles. We divide each plane equilateral triangle into a desired number of equilateral triangles, then project the intersections points to the unit sphere (see Figure 2.2).

It is natural and reasonable to divide the plane equilateral triangle into a number of small plane equilateral triangles of the same size. We partition all three sides into m equal sections and connect the corresponding partitioning points on each side with straight lines to create a refined plane triangle mesh.

The distribution of the spherical equilateral, isosceles, and general triangles within the initial spherical triangular areas is similar but not identical to the recursive construction. We do not have a simple formula as above. However, it is easy to identify the pattern: any triangle whose sides are part of the three (two) great circles of the same length is an equilateral (isosceles) triangle; the rest are general triangles. The analysis of the Voronoi cell mesh and its edges and vertices is the same as that of the recursive construction. We just replace 2^{2n} in the formula with m^2.

The major advantage of this construction is that all grid points within an initial spherical triangle are lined up on great circles. The other advantage of this construction is that we are no longer constrained by dyadic refinement that can only double the distance resolution (quadruple the point resolution). We can create a grid that is closer to the desired target resolution.

The major disadvantage of this construction is that the adjacent grid points along the sides of the initial spherical equilateral triangles are no longer equidistant. As a result, the shortest distance between adjacent grid points is shorter than that of the recursively constructed grid. Therefore, the ratio between the longest and shortest distances of adjacent grid points will be greater compared to the recursive approach.

Icosahedral-hexagonal grid mesh created with either construction follows the same overall trend: the regularity and size of the triangles and hexagons increase as these polygons get closer to the center of the initial equilateral triangles. This trend is caused by two facts of the icosahedral grid: the topological change of the Voronoi cell mesh from pentagons to hexagons at the initial vertices, and the different distances from the vertices and centers of the initial plane triangles to the sphere. More detailed and rigorous descriptions are presented in the next section.

For both constructions, the two key parameters we introduced earlier increase as the grid level n increases. Fortunately, as we will see in the next section, these parameters converge quickly to constant bounds.

3. Analysis of the geometric bounds of the icosahedral grid. In this section, we derive several geometric bounds of the icosahedral grid for both recursive and nonrecursive constructions. The first is the upper bound of the maximum ratio of the distances between the vertices of any single triangle in the triangle mesh; the second is the upper bound of the maximum ratio of the distances between adjacent grid points. From these two bounds, we derive a few other bounds that are of interest.

In the following, $\triangle(XYZ)$ denotes the spherical triangle XYZ on the unit sphere, and X and x denote the vertex/angle and corresponding arc length of the spherical triangle, respectively. $\mathcal{R}_*$ denotes the ratio bound.

3.1. The bound of the maximum ratio of the distances between the vertices of any single triangle in the grid mesh. First we show the bound for the icosahedral grid created with the recursive construction. We start with a few geometric propositions.

PROPOSITION 3.1. *Let $\triangle(ABC)$ be an acute spherical triangle, let a, b, and c be its corresponding sides, and let a_1, b_1, and c_1 be the sides of the inner spherical triangle after one bisection subdivision. If $a \geq b \geq c$, then $a_1 \geq b_1 \geq c_1$, and specifically, $\cos a_1/\cos b_1 = \cos\frac{a}{2}/\cos\frac{b}{2}$, $\cos a_1/\cos c_1 = \cos\frac{a}{2}/\cos\frac{c}{2}$, and $\cos b_1/\cos c_1 = \cos\frac{b}{2}/\cos\frac{c}{2}$.*

Proof. Let $\mathbf{X}$ denote the unit vector OX, where O is the origin of the three-dimensional ambient space and X is a vertex of a spherical triangle. With reference to Figure 3.1, we have

$$\begin{aligned}\cos a_1 &= \mathbf{D}\cdot\mathbf{E} = ((\mathbf{A}+\mathbf{B})\cdot(\mathbf{A}+\mathbf{C}))\eta_1 = (\mathbf{A}\cdot\mathbf{A}+\mathbf{A}\cdot\mathbf{C}+\mathbf{B}\cdot\mathbf{A}+\mathbf{B}\cdot\mathbf{C})\eta_1\\ &= (1+\cos b+\cos c+\cos a)\eta_1,\end{aligned}$$

where $\eta_1 = (4\cos\frac{c}{2}\cos\frac{b}{2})^{-1}$. Similarly,

$$\begin{aligned}\cos b_1 &= (\cos c+\cos b+1+\cos a)\eta_2,\\ \cos c_1 &= (\cos c+\cos b+\cos a+1)\eta_3,\end{aligned}$$

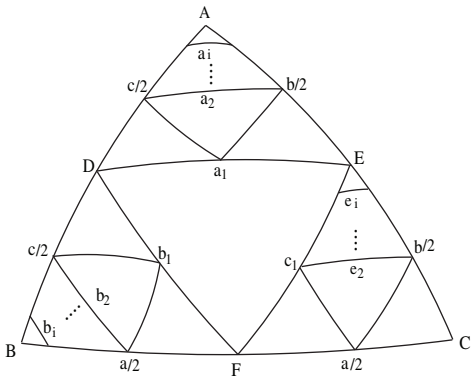

FIG. 3.1. *Recursive bisection of an acute spherical triangle. a_i, b_i, and e_i are great circle arcs that connect the bisecting points at different refinement levels.*

and $\eta_2 = (4\cos\frac{c}{2}\cos\frac{a}{2})^{-1}, \eta_3 = (4\cos\frac{b}{2}\cos\frac{a}{2})^{-1}$. Observing $\eta_1 \le \eta_2 \le \eta_3$ and dividing between the equations, we obtain the proposition. ∎

Proposition 3.1 gives the quantitative relationship between the side lengths of the inner triangle after one bisection refinement. Now we establish the quantitative relationship between the lengths of the sides corresponding to the largest angles in each of the three noncenter triangles after i bisection refinements.

PROPOSITION 3.2. *Let $\triangle(ABC)$ be an acute spherical triangle, and D, E, and F be the bisection points of the triangle sides. Let a_i, x_i, and y_i be the triangle sides corresponding to the largest angles of the subtriangles $\triangle(ADE)$, $\triangle(DBF)$, and $\triangle(EFC)$ at the ith bisection refinement. If $a \ge b \ge c$ and $a < \pi/2$, then $a_i \ge x_i, a_i \ge y_i, i = 1, 2, \ldots$.*

Proof. Let $b_1 \ge a/2$ and $a/2 \ge c_1$. We show that $a_i \ge b_i$ and $a_i \ge e_i$, $i = 1, 2, 3, \ldots$. Applying Proposition 3.1 to the triangles at vertices A and B after $k+1$ refinements, and letting $\zeta(x,k)$ denote $\cos(x/2^k)$, we have

$$\cos a_{k+1} = \Big(1 + \zeta(b,k) + \zeta(c,k) + \cos a_k\Big)\frac{1}{4}\zeta(c,k+1)^{-1}\zeta(b,k+1)^{-1},$$
$$\cos b_{k+1} = \Big(1 + \zeta(a,k) + \zeta(c,k) + \cos b_k\Big)\frac{1}{4}\zeta(c,k+1)^{-1}\zeta(a,k+1)^{-1}.$$

It follows that

(3.1)
$$\begin{aligned}\cos b_{k+1} - \cos a_{k+1} &= \frac{1}{2}\zeta(c,k+1)^{-1}\Big(\zeta(a,k+1) - \zeta(b,k+1)\Big)\\ &\quad + \frac{1}{4}\zeta(c,k+1)^{-1}\Big(\zeta(c,k) + \cos a_k\Big)\Big(\zeta(a,k+1)^{-1} - \zeta(b,k+1)^{-1}\Big)\\ &\quad + \frac{1}{4}\zeta(c,k+1)^{-1}\Big(\cos b_k - \cos a_k\Big)\zeta(a,k+1)^{-1}.\end{aligned}$$

Note that since $\cos a_k < \zeta(a,k)$, $a < \pi/2$, and $a \ge b \ge c$,

$$\begin{aligned}\Big(\zeta(c,k) + \cos a_k\Big)\zeta(a,k+1)^{-1}\zeta(b,k+1)^{-1} &\le \Big(1 + \zeta(a,k)\Big)\zeta(a,k+1)^{-1}\zeta(b,k+1)^{-1}\\ &= 2\zeta(a,k+1)\zeta(b,k+1)^{-1} \le 2,\end{aligned}$$

implying that the sum of the first and second terms of the right-hand side of (3.1) is less than or equal to 0. We also note that for $k \geq 1$ and $a \leq \pi/2$, $\frac{1}{4}\zeta(c, k+1)^{-1}\zeta(a, k+1)^{-1} < 1$. Thus, we have

$$\cos b_{k+1} - \cos a_{k+1} \leq \cos b_k - \cos a_k.$$

The equality holds when $a_i = b_i$, $i = 1, 2, 3, \ldots$, or

$$\cos b_{k+1} - \cos b_k \leq \cos a_{k+1} - \cos a_k.$$

That is, sequence $\{\cos a_i\}$ grows faster than $\{\cos b_i\}$. On the other hand, we note that $\cos a_1 \leq \cos b_1$ (Proposition 3.1), and both sequences $\{\cos a_i\}$ and $\{\cos b_i\}$ converge monotonically to one. Therefore, we have $\cos b_i \geq \cos a_i$, or $a_i \geq b_i$ $(i = 1, 2, 3, \ldots)$. Similarly, we can show $a_i \geq e_i$.

For the case that $b_1 \leq a/2$, or $a/2 \leq c_1$, the proof can also be obtained accordingly. □

PROPOSITION 3.3. *Let $\triangle(ABC)$ be an arbitrary acute spherical triangle, $a \geq b \geq c$. After any number of recursive bisection refinements, the spherical triangle in the triangle mesh with one vertex at A has the greatest side ratio.*

Proof. Now we argue that as we recursively bisect sides to create a finer triangle mesh within $\triangle(ABC)$, $a_i/(c/2^i)$ remains to be the maximum ratio among all triangles. From Proposition 3.1, we know that the inner triangle $\triangle(DEF)$ has a smaller side ratio and area compared to $\triangle(ABC)$; thus it can be excluded from further examination. Starting with spherical triangle $\triangle(ABC)$ after one bisection refinement (Figure 3.1), we perform one bisection refinement on each of the three noncenter subtriangles of $\triangle(ABC)$ and apply Proposition 3.2 to the triangle $\triangle(ABC)$. We get $a_2 \geq b_2$ and $a_2 \geq e_2$. After one more recursive bisection refinement, we apply Proposition 3.2 to the subtriangles $\triangle(ADE)$, $\triangle(DBF)$, and $\triangle(EFC)$. We get a_3, b_3, and e_3 as the longest sides of the three respective subtriangles. On the other hand, we know from the application of the same proposition to $\triangle(ABC)$ that $a_3 \geq b_3$ and $a_3 \geq e_3$; thus a_3 is the longest side among all subtriangles in $\triangle(ABC)$ that could possibly have larger side ratios. Carrying out the above two steps recursively to subtriangles, and noting $c/2^i$ to be the shortest side for all triangles in the triangle mesh after i refinements, we obtain the desired result. □

Since each initial spherical equilateral triangle is acute and its side lengths are less than $\pi/2$, and since largest angles of three noncenter subtriangles of the equilateral triangle are the angles at the initial vertices, from Proposition 3.3 we can conclude that the isosceles triangles with their top vertices being the initial vertices have the maximum side ratio.

For nonrecursive construction, we show in the following Proposition that the above claim is also true.

PROPOSITION 3.4. *In the triangle mesh created with nonrecursive construction, the isosceles triangles at the vertices of the initial equilateral triangles have the largest and smallest angles.*

Proof. First we find the relations between the sizes of the lower left angles in the triangle mesh (Figure 3.2). Let B_{ij} denote the lower left angle at vertex (i, j), where the ith and the jth great circles, which divide the initial equilateral triangle, intersect. It is straightforward to verify that $B_{ij} > B_{ij+1}$. Let us construct two isosceles triangles with one shared top angle and B_{ij} and B_{ij+1} as the base angles of the larger and smaller isosceles triangles, respectively (in Figure 3.2, triangles with thick lines). Apparently, the inequality holds. Similarly, we can show $B_{ij} > B_{i+1j}$.

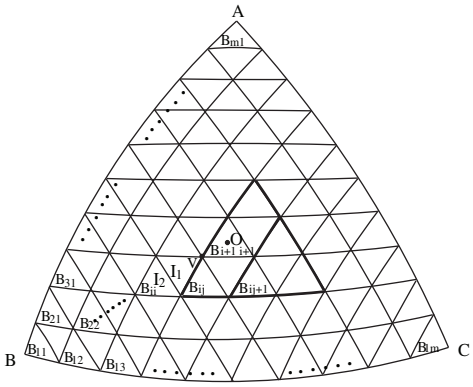

FIG. 3.2. *A triangle mesh created with nonrecursive construction, illustrating relations between angles. B_{ij} denotes the lower left angle of the triangle in the triangle mesh, O denotes the center, and I_1, I_2 are two exemplary isosceles triangles along the great circle between the center and the vertices of the initial equilateral triangle.*

To show that $B_{ii} > B_{i+1i+1}$, we observe that B_{i+1i+1} has a vertical angle V which is the top angle of the isosceles triangle I_1; I_1 shares the base with another isosceles triangle I_2 that has B_{ii} as top angle. Since isosceles I_1 has longer legs than I_2, $B_{ii} > V = B_{i+1i+1}$. Therefore, $\angle B$ is the largest angle for all lower left angles in the triangle mesh of the initial equilateral triangle area. By symmetry, $\angle A$ and $\angle C$ are also the largest angles for the top and lower right angles in the triangle mesh of the initial equilateral triangle. Based on the above angle size relations, exploring the vertical angles relations in the triangle mesh, we can further show that $\angle A$, $\angle B$, and $\angle C$ are the largest angles in the entire triangle mesh.

In a similar way, we can also show that angle B_{1m} and B_{m1} are the smallest angles in the entire triangle mesh. ∎

Now, we give the first bound for both constructions.

THEOREM 3.5. *The maximum ratio of the distances between the vertices of any triangle in the icosahedral grid mesh is bounded by $\mathcal{R}_1$,*

$$2\sin\frac{\theta_0}{2} \approx 1.175570,$$

where $\theta_0 = 2\pi/5$.

Proof. Since it has been shown that the maximum side ratios appear in the isosceles triangles at the initial vertices (Propositions 3.3 and 3.4), we can obtain the bound by computing the limit of the ratio between the longest and shortest sides of these isosceles triangles. Let x_n and θ_{bn} denote the length and a base angle of the isosceles triangle at grid point resolution n, where initial triangle sides are partitioned into m sectors; let x_0 and θ_0 be the side length and angle size of the initial equilateral triangle. From the spherical law of sines, we have

$$\sin x_n / \sin\frac{x_0}{m} = \sin\theta_0 / \sin\theta_{bn}.$$

Taking the limit of both sides as n goes to infinity, we get

$$\begin{aligned}\mathcal{R}_1 &= \lim_{n\to\infty} \frac{x_n}{x_0/m} \\ &= \lim_{n\to\infty} \frac{\sin x_n}{\sin(x_0/m)} = \lim_{n\to\infty} \frac{\sin\theta_0}{\sin\theta_{bn}} = \frac{\sin\theta_0}{\sin(\pi-\theta_0)/2} = 2\sin\frac{\theta_0}{2}.\end{aligned}$$ ∎

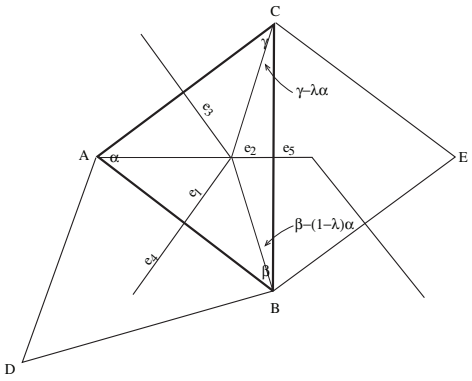

FIG. 3.3. *A Voronoi cell with the greatest edge ratio. Spherical triangle $\triangle ABC$ is a triangle with the greatest side ratio, and e_1, e_2, e_4, and e_5 are parts of the Voronoi cell edges.*

The ratio bound $\mathcal{R}_1$ is an important geometric bound for the icosahedral grid. It tells us how regular the triangle mesh is, locally, as the icosahedral grid approaches high resolution. In addition, it also provides the absolute lower bound of the maximum ratio of the distances between any adjacent grid points for any spherical grid based on the refinement of an icosahedron.

Related to the ratio bound $\mathcal{R}_1$ are the bound for the largest angles in the triangle mesh and the ratio bound of the longest and shortest edges of any Voronoi cell. We have the following results.

COROLLARY 3.6. *Let α_m be the largest angle in the icosahedral triangle mesh; then*

$$\alpha_m \leq \frac{2\pi}{5}.$$

Proof. For nonrecursive construction, we have shown in the proof of Proposition 3.4 that the largest angles are the angles of the initial equilateral, which is $2\pi/5$.

For recursive construction, suppose that there is a triangle $\triangle(ABC)$ that has $A > 2\pi/5$; then at the nth bisection refinement, we get a triangle $\triangle(AB^{(n)}C^{(n)})$. Assuming that the smallest angle in this triangle is $C^{(n)}$, when n approaches infinity, this angle must be less than $(\pi - 2\pi/5)/2 = 3\pi/10$. Thus, we will have $\lim_{n\to\infty} \sin A/\sin C^{(n)}$ exceeds $\mathcal{R}_1$, a contradiction. ∎

PROPOSITION 3.7. *Let α_m, γ_m be the largest and smallest angles of the triangle in the icosahedral triangle mesh with the greatest side ratio. Let $\mathcal{R}_e$ be the ratio bound of the longest and shortest Voronoi cell edges within a Voronoi cell, as the grid resolution n goes to infinity. Then*

$$\mathcal{R}_e = \lim_{n\to\infty} \frac{\cos\gamma_m}{\cos\alpha_m} \approx 1.90211.$$

Proof. With reference to Figure 3.3, we have a $\triangle(ABC)$, $\alpha \geq \beta \geq \gamma$, which contains three segments e_1, e_2, and e_3 of the corresponding Voronoi cell edges. By the definition of a Voronoi cell, for $0 < \lambda < 1.0$, we have

$$\beta - (1-\lambda)\alpha = \gamma - \lambda\alpha.$$

Solving for λ,

$$\lambda = \frac{\alpha - \beta + \gamma}{2\alpha}.$$

Thus,

$$\frac{\sin e_1}{\sin e_2} = \frac{\sin\left((1-\lambda)\alpha\right)}{\sin\left(\beta-(1-\lambda)\alpha\right)} = \frac{\sin\left((\alpha+\beta-\gamma)/2\right)}{\sin\left((\beta-\alpha+\gamma)/2\right)},$$
$$\frac{\sin e_3}{\sin e_2} = \frac{\sin\left(\lambda\alpha\right)}{\sin\left(\gamma-\lambda\alpha\right)} = \frac{\sin\left((\alpha-\beta+\gamma)/2\right)}{\sin\left((\beta-\alpha+\gamma)/2\right)}.$$

Since $\alpha \geq \beta \geq \gamma$, obviously $(\sin e_1/\sin e_2) \geq (\sin e_3/\sin e_2)$. As the grid resolution goes to infinity, it implies $e_1/e2 \geq e_3/e_2$.

We also observe a geometric fact: as the grid point resolution n goes to infinity, the neighboring triangles (such as $\triangle(ABC)$, $\triangle(ABD)$, and $\triangle(BCE)$ in Figure 3.3) approach congruence, with adjacent triangle pairs forming quadrilaterals with either reflection symmetry or 2-fold rotational symmetry. This implies that as the grid resolution n goes to infinity, e_4 and e_5 approach e_1 and e_2, respectively; thus

$$\mathcal{R}_e = \lim_{n\to\infty}\frac{e_1+e_4}{e_2+e_5} = \lim_{n\to\infty}\frac{e_1}{e_2} = \lim_{n\to\infty}\frac{\sin e_1}{\sin e_2} = \lim_{n\to\infty}\frac{\sin\left((\alpha+\beta-\gamma)/2\right)}{\sin\left((\beta-\alpha+\gamma)/2\right)} = \frac{\cos\gamma}{\cos\alpha}.$$

We obtain the bound when the ratio $\cos\gamma/\cos\alpha$ reaches maximum. For nonrecursive construction, since α_m and γ_m are the maximum and minimum angles of the whole triangle mesh, we have $\alpha = \alpha_m$ and $\gamma = \gamma_m$. For recursive construction, since $\alpha \leq 2\pi/5$ (Corollary 3.6), we assume $\alpha = 2\pi/5 - \delta_\alpha$ and $\gamma = 3\pi/10 - \delta_\gamma$, where δ_α and δ_γ are positive real numbers, such that $\sin\alpha/\sin\gamma \leq \mathcal{R}_1$. Thus, we have $\delta_\alpha > \delta_\gamma$ and

$$\frac{\cos\gamma}{\cos\alpha} = \frac{\cos\left(3\pi/10-\delta_\gamma\right)}{\cos\left(2\pi/5-\delta_\alpha\right)} \leq \frac{\cos\left(3\pi/10-\delta_\alpha\right)}{\cos\left(2\pi/5-\delta_\alpha\right)} \leq \frac{\cos\left(3\pi/10\right)}{\cos\left(2\pi/5\right)}.$$

From Theorem 3.5, we have $\alpha_m = 2\pi/5, \gamma_m = 3\pi/10$ as $n \to \infty$. Evaluating $\mathcal{R}_e$ at those values, we obtain the bound. ∎

3.2. The bound of the maximum ratio of the distances between adjacent grid points. First, we show the bound for recursive construction.

We start with a trivial claim.

PROPOSITION 3.8. *Let $\triangle(ABC)$ be a spherical triangle, and let $\triangle(DEF)$ be the spherical triangle whose vertices are the bisecting points of the sides a, b, and c of $\triangle(ABC)$. The sides of $\triangle(DEF)$ will always be longer than half of the corresponding sides of $\triangle(ABC)$.*

DEFINITION 3.9. *We say $\triangle(ABC)$ contains $\triangle(A'B'C')$ if all sides of $\triangle(ABC)$ are longer than or equal to those of $\triangle(A'B'C')$.*

PROPOSITION 3.10. *If $\triangle(ABC)$ contains $\triangle(A'B'C')$ and the maximum ratio between any sides of $\triangle(ABC)$ does not exceed $\sqrt{2}$, then after one bisection refinement all four subtriangles of $\triangle(ABC)$ contain the corresponding four subtriangles of $\triangle(A'B'C')$.*

Proof. Let a, b, c $(a \geq b \geq c)$ and a', b', c' $(a' \geq b' \geq c')$ denote the sides of $\triangle(ABC)$ and $\triangle(A'B'C')$, and let a_1, b_1, c_1 and a_1', b_1', c_1' denote the sides of their corresponding inner triangle (Figure 3.4). Let $\bar{x}$ denote the side of the underlying plane triangle corresponding to the side x. By definition, we have $a/2 \geq a'/2$, $b/2 \geq b'/2$, and $c/2 \geq c'/2$. Thus we just need to show $a_1 \geq a_1'$, $b_1 \geq b_1'$, and $c_1 \geq c_1'$.

We show $a_1 \geq a_1'$.

Since $b/2 \geq b'/2$ and $c/2 \geq c'/2$, we have $\cos\frac{b}{2} \leq \cos\frac{b'}{2}$ and $\cos\frac{c}{2} \leq \cos\frac{c'}{2}$. If $\angle M$ is acute (then $\angle N$ must be acute as well), then it is apparent that $\alpha' > \alpha$ implies

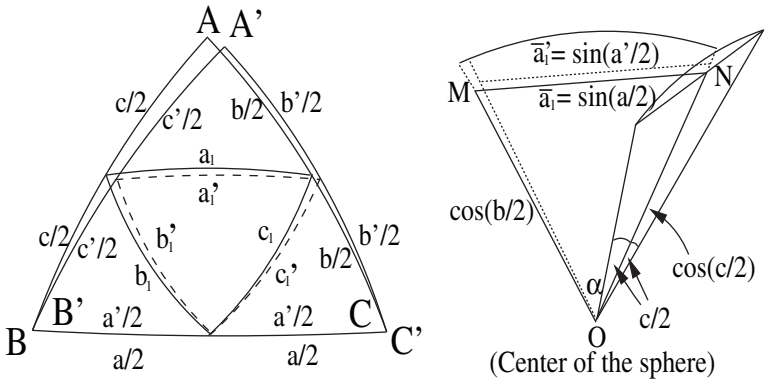

FIG. 3.4. *Preservation of containment relation during bisection subdivision of spherical triangles in icosahedral triangle mesh.*

$\bar{a_1'} > \bar{a_1}$ (law of sine for plane triangle), a contradiction. Thus, if $\angle M$ is acute, it must be that $\alpha \geq \alpha'$ or $a_1 \geq a_1'$.

Now we show that for the given constraints $\angle M$ cannot be obtuse. Suppose that $\angle M$ exceeds $\pi/2$, and let $b/2 = \lambda c/2$, $\lambda \geq 1.0$; then we have

$$\cos^2 \frac{\lambda c}{2} < \cos^2 \frac{c}{2} - \sin^2 \frac{a}{2} = \cos^2 \frac{c}{2} + \cos^2 \frac{a}{2} - 1 \leq 2\cos^2 \frac{c}{2} - 1, \text{ or}$$

$$\cos^2 \frac{c}{2} - \cos^2 \frac{\lambda c}{2} > 1 - \cos^2 \frac{c}{2}. \tag{3.2}$$

We consider the following limit and apply l'Hôpital's rule twice:

$$\lim_{c \to 0} \frac{\cos^2 \frac{c}{2} - \cos^2 \frac{\lambda c}{2}}{1 - \cos^2 \frac{c}{2}} = \lim_{c \to 0} \frac{\lambda^2 \cos(\lambda c) - \cos c}{\cos c} = \lambda^2 - 1.$$

On the other hand, this limit is strictly greater than 1 (3.2), and thus $\lambda > \sqrt{2}$, a contradiction.

Similarly, we also have $b_1 \geq b_1'$ and $c_1 \geq c_1'$. ∎

From Proposition 3.10 we have the following claim.

PROPOSITION 3.11. *Let $\triangle(ABC)$ and $\triangle(A'B'C')$ be two spherical triangles in the icosahedral triangle mesh created by recursive construction. If $\triangle(ABC)$ contains $\triangle(A'B'C')$, then all refinement triangles of $\triangle(ABC)$ at level i contain their corresponding refinement triangles of $\triangle(A'B'C')$ at level i.*

Proof. Applying Proposition 3.10 to both triangles and recursively to the subtriangles, noting that no triangle in the triangle mesh has a side ratio greater than $\mathcal{R}_1$ which is smaller than $\sqrt{2}$, we have the claim. ∎

From the above two claims, we can conclude that the longest triangle sides of the entire triangle mesh at any level of refinement are the sides of the center equilateral triangles, and the shortest triangle sides are those sides along the sides of initial equilateral triangles. Thus, to find the maximum ratio of the distances between adjacent grid points over the sphere, we just need to compute the relative length of the side of the center equilateral triangle to the distance between any adjacent grid points along the sides of the initial triangle.

To help establish the ratio upper bound at the limit of infinite bisection refinements, we give the following lemma.

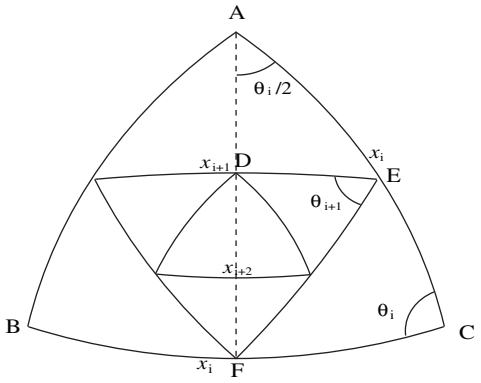

FIG. 3.5. *Recursive bisection of an equilateral triangle. Great circle $\overline{AD}$ and $\overline{AF}$ are perpendicular to great circles $\overline{DE}$ and $\overline{FC}$.*

LEMMA 3.12. *Let x_i be the arc length of the center spherical equilateral triangle at the ith bisection refinement from the initial spherical equilateral triangle. We have the following bound:*

$$\lim_{n\to\infty} \sin\frac{x_{t+n}}{2}\Big/\sin\frac{x_t}{2^{n+1}} < (\cos\tau)^{-1}\exp\left(\left(\cos\frac{\tau}{\varsigma}\right)^{-1}\tau^2\frac{\varsigma^2}{\varsigma^2-1}\right), \tag{3.3}$$

where t is a positive integer, $\varsigma = x_t/x_{t+1}$, $\tau = x_t/2$.

Proof. Let θ_i and x_i denote the angles and arc lengths of the equilateral triangles at the ith refinement (Figure 3.5). Applying Napier's rule to $\triangle(ADE)$ and $\triangle(AFC)$ (Figure 3.5) for $i \geq 0$, we have the following recursive relations:

$$\sin\frac{x_{i+1}}{2} = \sin\frac{\theta_i}{2}\sin\frac{x_i}{2} \tag{3.4}$$

and

$$\sin\theta_i = \cos\frac{\theta_i}{2}\Big/\cos\frac{x_i}{2}, \tag{3.5}$$

or

$$\sin\frac{\theta_i}{2} = \frac{1}{2}\Big(\cos\frac{x_i}{2}\Big)^{-1}. \tag{3.6}$$

It follows that

$$\sin\frac{x_{t+n}}{2} = 1/2^n\left(\prod_{i=0}^{n-1}\cos\frac{x_{t+i}}{2}\right)^{-1}\sin\frac{x_t}{2}, \quad n = 1, 2, \ldots, \tag{3.7}$$

$$\sin\frac{x_t}{2^{n+1}} = 1/2^n\left(\prod_{i=0}^{n-1}\cos\frac{x_t}{2^{i+2}}\right)^{-1}\sin\frac{x_t}{2}, \quad n = 1, 2, \ldots. \tag{3.8}$$

Dividing (3.7) by (3.8), we have

$$\sin\frac{x_{t+n}}{2}\Big/\sin\frac{x_t}{2^{n+1}} = \prod_{i=0}^{n-1}\cos\frac{x_t}{2^{i+2}}\Big/\prod_{i=0}^{n-1}\cos\frac{x_{t+i}}{2}. \tag{3.9}$$

Let $\varsigma = x_t/x_{t+1}$ ($2.0 - \epsilon < \varsigma < 2.0$, where ϵ is a small positive number which depends on t). Letting $\tau = x_t/2$ and $\epsilon_i = \tau/\varsigma^i - \tau/2^i$,

$$\begin{aligned}
\sin\frac{x_{t+n}}{2}\Big/\sin\frac{x_t}{2^{n+1}} &< \prod_{i=1}^{n}\cos\frac{\tau}{2^i}\Big/\left(\cos\tau\prod_{i=1}^{n}\cos\frac{\tau}{\varsigma^i}\right)\\
&= \prod_{i=1}^{n}\cos\left(\frac{\tau}{\varsigma^i}-\epsilon_i\right)\Big/\left(\cos\tau\prod_{i=1}^{n}\cos\frac{\tau}{\varsigma^i}\right)\\
&< \prod_{i=1}^{n}\left(\cos\frac{\tau}{\varsigma^i}+\sin\frac{\tau}{\varsigma^i}\sin\epsilon_i\right)\Big/\left(\cos\tau\prod_{i=1}^{n}\cos\frac{\tau}{\varsigma^i}\right)\\
&= (\cos\tau)^{-1}\prod_{i=1}^{n}(1+\rho_i),
\end{aligned}$$

where $\rho_i = \sin\frac{\tau}{\varsigma^i}\sin\epsilon_i/\cos\frac{\tau}{\varsigma^i} < \sin^2\frac{\tau}{\varsigma^i}/\cos\frac{\tau}{\varsigma^i} < (\cos\frac{\tau}{\varsigma})^{-1}(\frac{\tau}{\varsigma^i})^2$.

From a well-known relation between infinite product and infinite sum,

$$\prod_{i=1}^{n}(1+\rho_i) \le \exp\left(\sum_{i=1}^{n}\rho_i\right),$$

we have

$$\lim_{n\to\infty}\sin\frac{x_{t+n}}{2}\Big/\sin\frac{x_t}{2^{n+1}} < (\cos\tau)^{-1}\exp\left(\left(\cos\frac{\tau}{\varsigma}\right)^{-1}\tau^2\frac{\varsigma^2}{\varsigma^2-1}\right). \qquad \square$$

THEOREM 3.13. *For an icosahedral grid created with recursive bisection, the limit of the ratio of the longest and shortest distances between adjacent grid points exists. Furthermore, the limit is bounded by*

$$\left(\sin\frac{x_t}{2}\Big/\sin\frac{x_0/2}{2^t}\right)(\cos\tau)^{-1}\exp\left(\left(\cos\frac{\tau}{\varsigma}\right)^{-1}\tau^2\frac{\varsigma^2}{\varsigma^2-1}\right), \tag{3.10}$$

where t is a positive integer and $\varsigma = x_t/x_{t+1}$, $\tau = x_t/2$.

Proof. Following the recursive relations of (3.4) and (3.6), we have

$$\sin\frac{x_n}{2} = 1/2^n\left(\prod_{i=0}^{n-1}\cos\frac{x_i}{2}\right)^{-1}\sin\frac{x_0}{2}, \quad n = 1, 2, \ldots, \tag{3.11}$$

$$\sin\frac{x_0}{2^{n+1}} = 1/2^n\left(\prod_{i=0}^{n-1}\cos\frac{x_0}{2^{i+2}}\right)^{-1}\sin\frac{x_0}{2}, \quad n = 1, 2, \ldots. \tag{3.12}$$

The limit of the ratio between (3.11) and (3.12) as $n \to \infty$, if it exists, is the bound we are looking for. Rewriting the limit in two parts, we have

$$\lim_{n\to\infty}\sin\frac{x_n}{2}\Big/\sin\frac{x_0}{2^{n+1}} = \sin\frac{x_t}{2}\Big/\sin\frac{x_0/2}{2^t}\lim_{n\to\infty}\sin\frac{x_{t+n}}{2}\Big/\sin\frac{x_t}{2^{n+1}}. \tag{3.13}$$

Using Lemma 3.12, we have the proof. $\square$

From Theorem 3.13 we can obtain an accurate value of this bound with the following procedure. We first compute the expression $\sin\frac{x_t}{2}/\sin\frac{x_0/2}{2^t}$ numerically

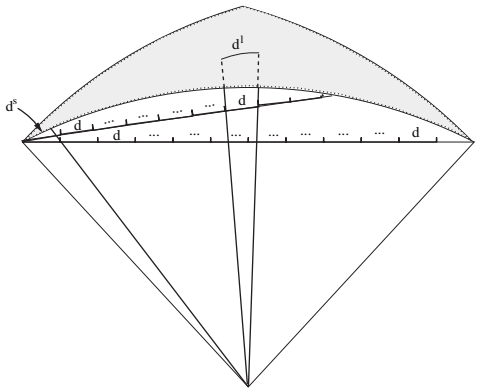

FIG. 3.6. *Longest and shortest distances between adjacent grid points for nonrecursive construction. In the figure d is the distance between adjacent vertices of the plane triangle mesh, and d^s and d^l are the distances between adjacent vertices of the spherical triangle mesh on the sphere, at the center and the vertices of the initial spherical equilateral triangle, respectively.*

with (3.4) and (3.6). Then we multiply it by the bound for the infinite product (the right-hand side of inequality (3.3)) to get a bound for the limit. The bigger the t, the tighter the bound. For all practical purposes, for $t = 10$, the computed bound, which equals $1.19511377 \cdot 1.000000805 = 1.195114732$, provides more than enough accuracy.

Now, we give the same ratio bound for the icosahedral grid created by nonrecursive construction.

THEOREM 3.14. *For an icosahedral grid created with nonrecursive construction, the limit of the ratio of the longest and shortest distances between adjacent grid points exists and is bounded by*

$$\left(\cos^2\frac{x_0}{2} - \tan^2\frac{\pi}{6}\sin^2\frac{x_0}{2}\right)^{-1/2}\left(\cos\frac{x_0}{2}\right)^{-1} \approx 1.479348,$$

where x_0 is the arc length of a side of the initial equilateral triangles, which equals $2\cos^{-1}(1/2\csc\frac{\pi}{5})$.

Proof. Let m be the number of partitions along the sides of the initial equilateral triangles. Let d be the distance between adjacent grid points on the plane (which is a constant for a given m), and let d^l and d^s be the longest and shortest distances between any adjacent grid points on the sphere (Figure 3.6).

We have the following limits:

$$\lim_{m\to\infty}\frac{d^l}{d} = \left(\cos^2\frac{x_0}{2} - \tan^2\frac{\pi}{6}\sin^2\frac{x_0}{2}\right)^{-1/2} \tag{3.14}$$

and

$$\lim_{m\to\infty}\frac{d^s}{d} = \cos\frac{x_0}{2}. \tag{3.15}$$

Dividing (3.14) by (3.15), we obtain the result. ∎

Let us call this ratio bound for both constructions $\mathcal{R}_2$. The numerical experiments show that for either construction, the ratio converges to its bound rather quickly. Thus this bound is a good measure for an icosahedral grid at most practical grid resolutions.

With this ratio bound, we can also calculate the ratio bound for the areas of the largest and smallest Voronoi cells. Let $\mathcal{R}_a$ denote this area ratio bound, n the number of the grid points, and $A_{n,vl}$ and $A_{n,vs}$ the areas of the largest and smallest Voronoi cells among all n Voronoi cells. As n approaches infinity, the obvious area ratio bound $\mathcal{R}_a = \lim_{n\to\infty} A_{n,vl}/A_{n,vs} = \mathcal{R}_2^2$, where $A_{n,vl}$ and $A_{n,vs}$ are the areas of largest and smallest regular spherical hexagons with their apothems being half of the greatest and smallest distances between adjacent grid points, respectively. This is due to the fact that a regular hexagon is smaller than a regular pentagon with the same apothem. However, we observe that the smallest spherical hexagons in the grid mesh (those nearest to the initial vertices and surrounding the pentagons) are not regular and have their area approach $\tan(\pi/5) + 2\sin^2(\pi/5)\tan(\pi/10)$ when normalized by the square of the shortest distance between any adjacent grid points. This area is actually greater compared to that of the surrounded spherical pentagons, which approaches $1.25 \cdot \tan(\pi/5)$ when normalized by the same distance square. Thus, $A_{n,vs}$ should be the area of one of the pentagons at grid point resolution n. Therefore, we have the following tighter bound:

$$\mathcal{R}_a = \lim_{n\to\infty} \frac{A_{n,vl}}{A_{n,vs}} = \frac{6\tan(\pi/6)}{5\tan(\pi/5)}\mathcal{R}_2^2 \approx 0.953585367\mathcal{R}_2^2.$$

4. Proposed procedure for modified icosahedral grids. In this section we propose two modified construction algorithms for icosahedral grids, one for recursive construction and the other for nonrecursive construction. The modification to the recursive construction improves the maximum ratio of the distances between adjacent grid points. The modification to the nonrecursive construction improves the regularity of hexagonal Voronoi cells.

To quantify the regularity of the Voronoi cells, we use the maximum and average ratio of the longest and shortest length of the Voronoi cell edges to measure the local extreme and overall regularity of the Voronoi cell mesh.

4.1. Modification to the classic recursive construction. In the classic recursive construction, at any level, the sides of the triangle are bisected and the middle points as new vertices (anchor points) are interconnected to create four subtriangles. In this way, a subtriangle at the center of the triangle tends to be larger than the rest of the three subtriangles. Since the construction is recursive, the grid mesh created will have many local minimum and maximum triangles, and the center equilaterals, relative for the grid level, will get bigger at each recursion, as has been shown in the analysis in the previous section. To alleviate this problem of unevenness, we propose a new algorithm to compute the anchor points. Observe that each new grid point inside the outer triangle is actually related to three great circles ($\overline{DE}$, $\overline{GH}$, and $\overline{JK}$ in Figure 4.1). Intuitively it will be better to assign the anchor point to the place which best accommodates all three great circles. Instead of just using the bisection point of an inner triangle side ($\overline{DE}$), we in addition compute two trisection points of two other great circles ($\overline{GH}$ and $\overline{JK}$), which connect the two pairs of quad-section points of the outer triangle. Together with the bisection point of an inner triangle side, we now have three points to determine the location of the new grid point. We can either compute the average of the three points or the Fermat point of the triangle defined by these three points and use it as a new anchor point.

As a result of this modification, the ratio of the longest and the shortest distance between adjacent grid points is improved by about 2% together with some marginal improvements to the other parameters (Table 4.1, with three-point average algorithm).

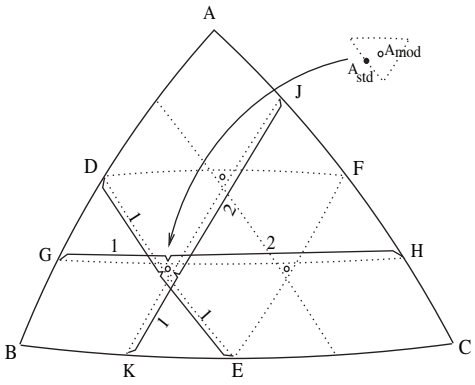

FIG. 4.1. *Recursive subdivision of triangle, new anchor point computation. The dotted lines are great circles, and D, E and G, H, J, K are bisecting points at two consecutive refinement levels. The upper right is the enlarged portion of the pointed area; the small dots A_{std} and A_{mod} are the anchor locations for standard construction and modified recursive construction, respectively.*

TABLE 4.1
Comparison between basic and modified recursive construction grid.

Ratios of the max. and min. distances between adjacent grid points							
Grid level	3	4	5	6	7	8	9
Standard	1.19105	1.19409	1.19486	1.19505	1.19510	1.195113	1.195114
Modified	1.17311	1.17496	1.17542	1.17554	1.17557	1.17558	1.17560
Max. ratios of the longest and shortest edge lengths within each Voronoi cell							
Standard	1.83556	1.88500	1.89780	1.90104	1.90184	1.90205	1.90210
Modified	1.76923	1.85845	1.88917	1.89847	1.90112	1.90185	1.90204
Average ratio of the longest and shortest edge lengths of each Voronoi cell							
Standard	1.42388	1.45590	1.46881	1.47370	1.47555	1.47628	1.47660
Modified	1.40393	1.41578	1.41538	1.41138	1.40786	1.40545	1.40402
Average distances between adjacent grid points (with earth radius 6371.220 km)							
Standard	961.255	481.137	240.632	120.324	60.1630	30.0817	15.0408
Modified	961.082	481.042	240.584	120.300	60.1508	30.0757	15.0378

We note that this ratio is close to the ratio bound $\mathcal{R}_1$, the bound of the maximum ratio of the distances between the vertices of any triangle, $2\sin(\theta_0/2) \approx 1.17557$. In other words, this improved ratio is close to the absolute lower bound for any icosahedral grids.

4.2. Modification to the nonrecursive construction. The icosahedral grid created with nonrecursive construction (great circle construction) measures well in terms of many geometric properties. It improves the regularity of the Voronoi cells and has a smaller average distance between adjacent grid points compared with the recursively constructed grid. One main disadvantage of this construction is that it increases the ratio of the longest and shortest distances between adjacent grid points.

Compared with the grid mesh postprocessed by the spring-dynamics optimization procedure [17], this grid has a better ratio of the longest and shortest distances between adjacent grid points, but a worse regularity measure.

We observe that due to the uniform projection of the triangle mesh to the sphere, the triangle mesh near the vertices of the equilateral triangle is compressed toward these vertices. This compression helps to smooth the transition caused by the topological change from a regular pentagon to hexagons, which is inevitable in an icosahedral-

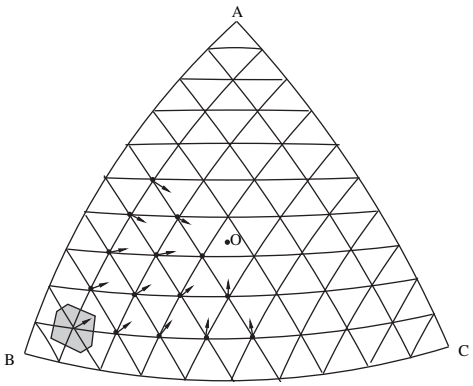

FIG. 4.2. *Modifications to the nonrecursive construction, nudging the points near the vertices of the initial equilateral triangle toward the center O. Shaded area is an exemplary Voronoi cell.*

hexagonal grid mesh. However, this compression also causes two problems: (a) the triangles near the center are expanded, while those near the vertices are shrunk, which increases the ratio of the longest and shortest distances between adjacent grid points; (b) it appears that the interior grid points near the initial vertices are overcompressed due to this compression, causing the Voronoi cells in the area to be less regular (Figure 4.2), which affects the regularity measures of the grid.

We propose the following modification to the nonrecursive construction to alleviate the above problems. Before we project each internal point to the sphere, we apply a function to its coordinate to "nudge" the points toward the center of the plane equilateral triangle, with the amount of this nudging depending on the point location. Let $\mathbf{O} \in R^3$ be the center of the plane equilateral triangle, $\mathbf{A}$, $\mathbf{B}$, $\mathbf{C} \in R^3$ be the three vertices of the initial equilateral triangle, $\mathbf{p} \in R^3$ be an internal grid point on the plane equilateral triangle, $\mathbf{E} \in R^3$ be the projection of $\mathbf{p}$ to the closest side of the plane equilateral triangle, and $\mathbf{V_1}, \mathbf{V_2} \in \{\mathbf{A}, \mathbf{B}, \mathbf{C}\}$ be the two vertices of the closest side. The notation $\|.\|$ denotes Euclidean norm. The "nudging" of point $\mathbf{p}$ is expressed as

$$\mathbf{p} = (1 - w(\mathbf{p}))\mathbf{p} + w(\mathbf{p})\mathbf{O}, \tag{4.1}$$

where

$$\begin{aligned} w(\mathbf{p}) &= \alpha_1 r_1(\mathbf{p})/(r_1(\mathbf{p}) + \alpha_2 r_2(\mathbf{p})), \\ r_1(\mathbf{p}) &= \|\mathbf{A} - \mathbf{O}\|/\|\mathbf{p} - \mathbf{O}\|, \quad r_2(\mathbf{p}) = \|\mathbf{A} - \mathbf{B}\|/\|\mathbf{p} - \mathbf{E}\|. \\ \mathbf{E} &= \mathbf{V_1} + t(\mathbf{V_2} - \mathbf{V_1}), \quad t = (\mathbf{p} - \mathbf{V_1}) \cdot (\mathbf{V_2} - \mathbf{V_1})/\|\mathbf{V_2} - \mathbf{V_1}\|^2. \end{aligned}$$

Here α_1 and α_2 are specified parameters.

In the formula, $w(p) \ll 1$ is a weight function directly proportional to the actual amount of nudging. The amount of nudging increases as the grid point $\mathbf{p}$ moves closer to the vertices of the initial triangle and the distance from $\mathbf{p}$ to the closest side of the initial plane triangle remains the same. This helps to improve the regularity of the Voronoi cell in the local area and to make the transition of the grid points across the adjacent initial triangle smoother. The amount of nudging also increases as the grid point $\mathbf{p}$ gets closer to the center of the initial plane triangle from the sides. This helps to reduce the maximum ratio of the distances between adjacent grid points, since the

TABLE 4.2
Comparison between the basic and modified nonrecursive construction grids.

Ratios of the max. and min. distances between adjacent grid points							
Grid level	3	4	5	6	7	8	9
Standard	1.37902	1.42861	1.45387	1.46659	1.47296	1.47616	1.47775
Modified	1.34609	1.39493	1.42073	1.43402	1.44125	1.44555	1.44892
Max.l ratios of the longest and shortest edge lengths within each Voronoi cell							
Standard	1.57602	1.72604	1.81024	1.85513	1.87835	1.89016	1.89612
Modified	1.49135	1.58007	1.62062	1.64297	1.65924	1.67386	1.68728
Average ratios of the longest and shortest edge lengths of the Voronoi cell							
Standard	1.17895	1.19115	1.19432	1.19468	1.19456	1.19442	1.19433
Modified	1.13852	1.13943	1.13935	1.13704	1.13533	1.13457	1.13452
Average distances between adjacent grid points (with earth radius 6371.220 km)							
Standard	957.133	478.955	239.526	119.769	59.8852	29.9427	14.9714
Modified	957.282	479.073	239.591	119.800	59.8997	29.9491	14.9742

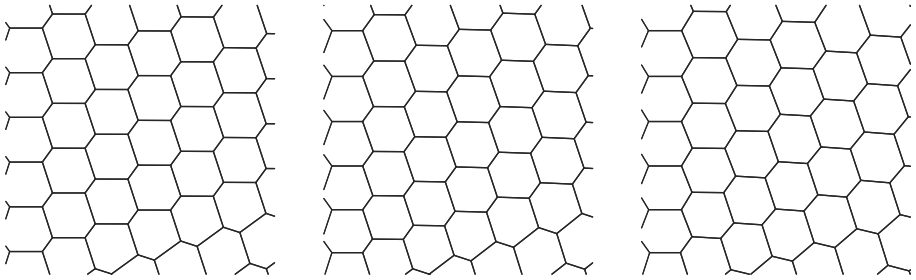

FIG. 4.3. *Voronoi cells in a region near a vertex of the initial equilateral triangle. Left: Standard recursive construction. Middle: Standard nonrecursive construction. Right: Modified nonrecursive construction. The modified nonrecursive construction produces a more regular Voronoi cell mesh compared with the meshes produced by the other two constructions.*

nudging makes the center triangles a little smaller. Parameter α_1 controls the overall nudging amount, while α_2 adjusts the penalty to the nudging amount for the grid point $\mathbf{p}$ being close to the sides of the initial plane triangle.

Table 4.2 shows the maximum and average ratios of the longest and shortest edge lengths of all Voronoi cells for basic nonrecursive construction and its modified version. (The two parameters α_1 and α_2 vary from 0.025 to 0.02 and 0.08 to 0.1 roughly linearly for the icosahedral grids at grid level 3 to 9.)

The modified construction algorithm creates a more regular grid in terms of our regularity measure, while improving the ratio of the longest and shortest distances between adjacent grid points. The maximum ratio of the longest and shortest edge lengths within each Voronoi cell still increases with the grid level and approaches the theoretical bound $\mathcal{R}_e$, however, at a slower pace. The corresponding average ratio which measures the general regularity of the Voronoi cells improves by more than 0.05 to about 1.13. This is a significant improvement, considering that the apparent optimal value for this ratio is 1.0. The average distance between adjacent grid points increases by a small amount ($< 0.1\%$), which reflects the fact that slight adjustment of the grid points causes internal grid points to be away from the intersection points of the three great circles. Figure 4.3 compares the Voronoi cell meshes near a vertex of the initial equilateral triangle from three algorithms: standard recursive, standard nonrecursive, and modified nonrecursive constructions. (The mesh of the modified recursive construction is very similar to that of the standard recursive construction and visually identical.)

Compared to widely used optimization methods for the icosahedral grid, this algorithm offers several unique features. First, it is noniterative and thus much more efficient. The algorithm adds very little extra computation to the standard construction method and creates the grid mesh in one step. Without a slowly convergent computation to globally minimize the cost function, this new method can be used to create a high resolution icosahedral grid dynamically. Second, the modified grid has a smaller average distance between adjacent grid points and a maximum ratio of distances between adjacent grid points that is comparable to those of other iterative optimization algorithms [17, 2]. At the same time, numerical experiments (in the next section and in [6]) have shown that the modified grid produces simulation results very similar to those produced by the icosahedral grids opimized with iterative methods. Third, with two parameters to tune, the new algorithm provides some flexibility in controling the trade-off between the regularity of the local grid mesh and the uniformity of the entire grid. In addition, it should be noted that neither the formula nor the two parameters (α_1, α_2) have been optimized yet. For example, it would increase the minimum distance between adjacent grid points if the grid points along each side of the initial triangles were also nudged from two ends toward the middle of the side. We leave the optimization of the proposed modification to future work.

5. Numerical experiments on icosahedral grid regularity. In this section, the icosahedral grid regularity is tested with lee wave simulations obtained with a finite-volume shallow water model (SWM). The model is discretized on the icosahedral grids from four construction algorithms, namely, the standard recursive algorithm, modified recursive algorithm, standard nonrecursive algorithm, and modified nonrecursive algorithm. The regularity measures for these four grids at different resolutions are listed in Tables 4.1 and 4.2. The nonlinear lee wave test case is one of the standard SWM test cases described in [18] typically used to evaluate the impact of different algorithms on numerical weather prediction models. The SWM used in this study, described in [6], is discretized with finite-volume operators whose stencil points are defined on the icosahedral grid. These stencil points are indexed through a predefined look-up table so that the model can be used to conveniently test different icosahedral grids without changing model coding except for the predefined table. (See [6] for details.)

In this test case, lee waves are generated by zonal (east-west) flow impinging on an isolated mountain. The initial zonal velocity and height fields are specified as follows:

$$\phi = gh_0 - \left(a\Omega u_0 + \frac{u_0^2}{2}\right)(-\cos\lambda\cos\theta\sin\alpha + \sin\theta\cos\alpha)^2,$$
$$u = u_0(\cos\theta\cos\alpha + \cos\lambda\sin\theta\sin\alpha),$$
$$f = 2\Omega(-\cos\lambda\cos\theta\sin\alpha + \sin\theta\cos\alpha),$$

where g is the gravitational constant of 9.8, a the earth radius in meters (6371220), α a real number parameter, Ω the angular speed of the earth rotation $(7.292 \cdot 10^{-5})$, and f the Coriolis parameter used in the analytical solution. The mountain profile is given as

$$h_s = h_{s0}\Big(1 - \frac{r}{R}\Big),$$

where λ and θ denote longitude and latitude, respectively, $h_{s0} = 2000$m, $R = \frac{\pi}{9}$, and $r^2 = \min[R^2, (\lambda - \lambda_c)^2 + (\theta - \theta_c)^2]$. The center of the mountain is chosen as $\lambda_c = \frac{\pi}{2}$ and $\theta_c = \frac{\pi}{6}$.

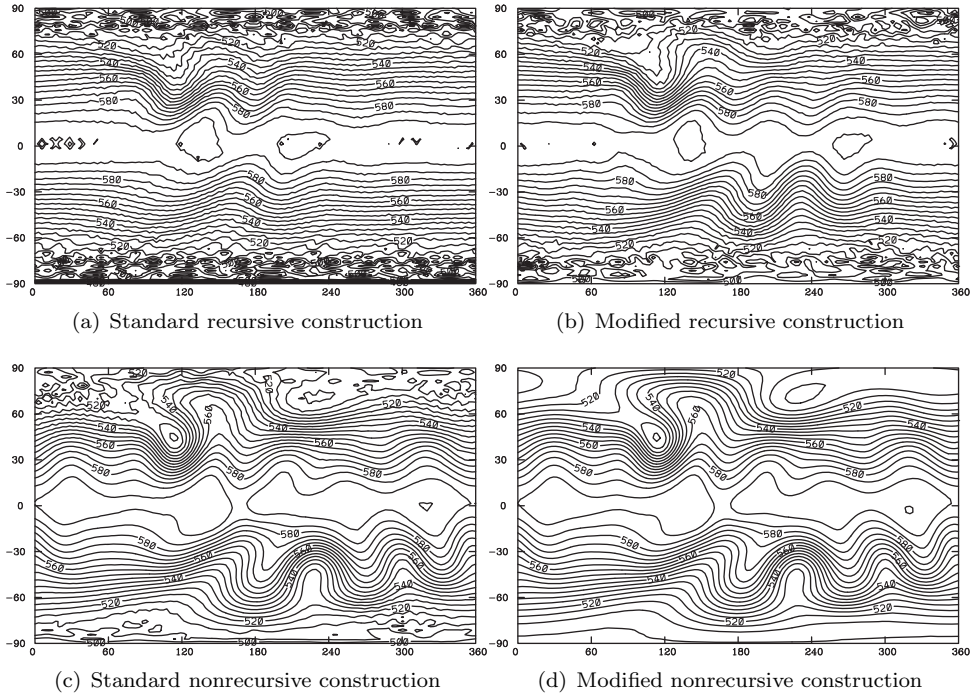

(a) Standard recursive construction (b) Modified recursive construction

(c) Standard nonrecursive construction (d) Modified nonrecursive construction

FIG. 5.1. *The height fields simulated using the same SWM formulated on the* (a) *standard recursive,* (b) *modified recursive,* (c) *standard nonrecursive, and* (d) *modified nonrecursive icosahedral grids. Figures* (a) *and* (b) *show, respectively, the lee wave solutions on day* 6 *and* 9*, while* (c) *and* (d) *show the solutions on day* 15*. The contour interval,* 50 *m, is the same in all height fields.*

The parameter values used in this study are $\alpha = 0$, $h_0 = 5960$ m, and $u_0 = 20$ m/s. With α being zero, the initial height field is a function of latitude only, and the maximum height is found along the equator. The zonal wind field is in geostrophic balance with the height field. The meridional wind is zero initially. The lee wave solution is obtained by integrating the finite-volume model with the zonal flow initial condition for 15 days in order to evaluate the impact of grid sensitivity on the numerical accuracy of the lee wave solution. Figure 5.1 shows height fields simulated on the modified and standard icosahedral grids, two from basic constructions and two from their modified versions, at the resolution of grid level 5.[1] Figures 5.1(a)–5.1(d) correspond, respectively, to the standard recursive, modified recursive, standard nonrecursive, and modified nonrecursive constructions analyzed in the previous sections. The regularity measures of these grids are shown in Tables 4.1 and 4.2. The regularities of nonrecursive grids are better than those of the recursive grids. At the same time, the modified grids, either recursive or nonrecursive, have better regularity than the standard grids. Note that the grid regularity used in the lee wave simulations improves from Figure 5.1(a) to 5.1(d).

In the lee wave test, it is required to integrate the numerical solution for 15 days, which is the standard time period for the test case. However, numerical solutions obtained with the standard and modified recursive grids blew up shortly after day 6 and

[1] All of the figures shown in this section are linearly interpolated from the icosahedral grid to the regular latitude/longitude grid for display purposes.

9 as shown in Figures 5.1(a) and 5.1(b). The height fields in Figure 5.1(a) and 5.1(b) exhibit noises superimposed on the lee wave solution, especially at high latitudes. These noises are caused by slight irregularities in the recursively constructed icosahedral grids. These grid noises eventually dominate true solutions, and the solutions become unstable before they complete the 15-day model integration. The standard recursive grid with worse regularity measure than the modified recursive grid produces more noise and thus less stable integration than the modified grid.

In contrast, the simulations with the nonrecursive grids successfully complete 15-day integrations with the results shown in Figures 5.1(c) and 5.1(d), respectively, for the standard and modified grids. The height field at day 15 in Figure 5.1(c) exhibits substantial noises in high latitudes, indicating that slight grid irregularities near the pole cause the noises in high latitudes where strong vorticities exist in the lee wave solution. On the other hand, the numerical solution shown in Figure 5.1(d) with the modified nonrecursive grid is free of high-latitude noises which exist in the standard nonrecursive grid with a slightly worse grid regularity. Figure 5.1(d) shows a smooth height field very similar to that shown in Figure 7a of [6], the same experiment with the spring dynamics optimized grid. The height field shown in Figure 5.1(d) is also found to be very similar to several other published results, e.g., Figure 4 in [7], Figure 6 in [15], on the grids optimized with different numerical algorithms.

Figures 5.1(a)–(d) confirm that the icosahedral grid tends to introduce noises associated with the grid imprint for sensitivity test [5]. They also convincingly demonstrate that improved grid regularities lead to improved lee wave solutions. It is worth pointing out that this test case is particularly sensitive to the regularity of the grid and the test result by no means suggests that one should use only the icosahedral grid with the best regularity. For applications extremely sensitive to the regularity of the grid cells, the modified nonrecursive grid, for example, might be a good choice. On the other hand, many real-world applications are not as sensitive to the grid regularity as the test case. For these applications, the modified recursive grid could be a proper choice because it has the best uniformity measure, which could help to maximize the time step of the simulation.

6. Conclusion. In this paper, we derived some important geometric bounds of the icosahedral grid. These bounds helped us understand the geometric properties of the grid as its resolution increases. They directly defined regularity and uniformity of the icosahedral grid. Two basic construction methods for the icosahedral grid were investigated. In an effort to improve the geometric properties, two modifications to the two basic constructions were proposed.

A numerical experiment was carried out to compare the modified grids to the grids from basic constructions. The results clearly demonstrated the improved numerical properties of the modified grids.

In summary, we have the following remarks:

(a) The two basic constructions have pros and cons of their own. According to our analysis and the derived bounds, both constructions create grid meshes with a relatively small ratio of the longest and shortest distances between adjacent grid points, even at high grid resolution. The main disadvantage of the recursive construction is the existence of local minimum and maximum triangles which undermines the grid's regularity. The main disadvantage of the nonrecursive construction is that adjacent points along the sides of the initial 20 spherical equilateral triangles are no longer equidistant, which in turn implies smaller grid distance near the vertices of those equilateral triangles and a larger ratio of the adjacent grid point distances.

(b) The icosahedral grids from both basic constructions are more uniform compared to most other grid meshes (cubed-sphere grid [11, 12] and composite grid ([4], for example) on the sphere. Moreover, modifications can be made to further improve the geometric properties of the icosahedral grid. The proposed modification to the recursive construction improves the ratio of the longest and shortest distances between adjacent grid points. Although the improvement is relatively modest, the ratio we have achieved approaches the lower bound for the icosahedral grid. In other words, it is close to the optimal value. The modification to the nonrecursive construction is effective in improving our regularity measures of the grid. The resultant grids from both modifications show better geometric statistics and numerical properties.

(c) Compared to other grid optimization methods, the proposed direct methods are efficient in computation and flexible in control. The proposed direct modification to the nonrecursive construction improves grid geometric properties similarly to what other iterative optimization schemes such as spring dynamic methods have achieved. This method provides an interesting alternative to the iterative approaches. With two parameters to tune (and possible further improvement to the formula), the method allows the users of the icosahedral grid to obtain a good compromise between larger time step and smaller truncation errors.

Acknowledgments. The authors thank Drs. Yuanfu Xie and Dezso Devenyi for their insightful discussions and comments, and Drs. Rainer Bleck and John Brown for their suggestions on the presentation of the article. The authors would also like to thank the anonymous reviewers for their constructive comments. Ann Reiser has kindly provided editorial reviews for the manuscript.

REFERENCES

[1] J. R. Baumgardner and P. O. Frederickson, *Icosahedral discretization of the two-sphere*, SIAM J. Numer. Anal., 22 (1985), pp. 1107–1115.

[2] R. Heikes and D. A. Randall, *Numerical integration of the shallow-water equations on a twisted icosahedral grid. Part* II: *A detailed description of the grid and an analysis of numerical accuracy*, Mon. Wea. Rev., 123 (1995), pp. 1881–1887.

[3] R. Heikes and D. A. Randall, *Numerical integration of the shallow-water equations on a twisted icosahedral grid. Part* I. *Basic design and results of tests*, Mon. Wea. Rev., 123 (1995), pp. 1862–1880.

[4] A. Kageyama and T. Sato, *"Yin-Yang" grid: An overset grid in spherical geometry*, Geochem. Geophys. Geosyst., 5 (2004), Q09005.

[5] P. H. Lauritzen, C. Joblonowski, A. Taylor, and R. D. Nair, *Rotated versions of the Joblonowski steady-state and baroclinic wave test cases: A dynamical core intercomparison*, J. Adv. Model. Earth Syst., 2 (2010), 15.

[6] J.-L. Lee and A. E. MacDonald, *A finite-volume icosahedral shallow-water model on a local coordinate*, Mon. Wea. Rev., 137 (2009), pp. 1422–1437.

[7] S. J. Lin and R. B. Rood, *An explicit flux-form semi-Lagrangian shallow-water model on the sphere*, Quart. J. Roy. Meteor. Soc., 123 (1997), pp. 2477–2498.

[8] D. Majewski, D. Liermann, P. Prohl, B. Ritter, M. Buchhold, T. Hanisch, G. Paul, and W. Wergen, *The operational global icosahedral-hexagonal gridpoint model GME: Description and high-resolution tests*, Mon. Wea. Rev., 130 (2002), pp. 319–338.

[9] Y. Masuda and H. Ohnishi, *An integration scheme of the primitive equations model with an icosahedral-hexagonal grid system and its application to the shallow water equations*, in Short- and Medium-Range Numerical Weather Prediction, T. Matsuno, ed., Japan Meteorological Society, Tokyo, 1986, pp. 317–326.

[10] H. Miura and M. Kimoto, *A comparison of grid quality of optimized spherical hexagonal-pentagonal geodesic grids*, Mon. Wea. Rev., 133 (2005), pp. 2817–2833.

[11] W. M. Putman and S.-J. Lin, *Finite-volume transport on various cubed-sphere grids*, J. Comput. Phys., 227 (2007), pp. 55–78.

[12] W. M. Putman and S.-J. Lin, *A finite-volume dynamical core on the cubed-sphere grid*, in Proceedings of the 3rd International Conference on Numerical Modeling of Space Plasma Flows: Astronum-2008, Astronomical Society of the Pacific Conference Series 406, 2009, pp. 268–276.

[13] R. Sadourny, A. Arakawa, and Y. Mintz, *Integration of the non-divergent barotropic vorticity equation with an icosahedral-hexagonal grid for the sphere*, Mon. Wea. Rev., 96 (1968), pp. 351–356.

[14] J. Steppeler, P. Ripodas, B. Jonkheid, and S. Thomas, *Third-order finite-difference schemes on icosahedral-type grids on the sphere*, Mon. Wea. Rev., 136 (2008), pp. 2683–2698.

[15] J. Thuburn, *A PV-based shallow-water model on a hexagonal-icosahedral grid*, Mon. Wea. Rev., 125 (1997), pp. 2328–2347.

[16] H. Tomita, K. Goto, and M. Satoh, *A new approach to atmospheric general circulation model: Global cloud resolving model NICAM and its computational performance*, SIAM J. Sci. Comput., 30 (2008), pp. 2755–2776.

[17] H. Tomita, M. Tsugawa, M. Satoh, and K. Goto, *Shallow water model on a modified icosahedral geodesic grid by using spring dynamics*, J. Comput. Phys., 174 (2001), pp. 579–613.

[18] D. L. Williamson, J. B. Drake, J. J. Hack, R. Jakob, and P. N. Swarztrauber, *A standard test set for numerical approximations to the shallow water equations in spherical geometry*, J. Comput. Phys., 102 (1992), pp. 221–224.